Advances in Turbulence Research-2002, pp. 115-135
Seoul Nat'l Univ., Seoul, Korea, April 27, 2002

Recent progress in active feedback control of wall turbulence

By NOBUHIDE KASAGI†

Department of Mechanical Engineering, The University of Tokyo, Tokyo 113-8656, JAPAN

(Received 13 April 2002)

The research effort toward the active feedback control of wall-bounded turbulence at the University of Tokyo is surveyced. Both control algorithm and hardware element have been intensively studied to be integrated in a future control unit for various applications. In order to highlight the progress, three studies are briefly described. Unlike channel flow simulation employed in previous investigations, the so-called active cancellation control is tested in a turbulent pipe flow with the control applied on the wall entirely and partially. The drag reduction rate achieved is comparable to that in the plane channel flow, and that, when partially controlled, the reduction rate is nearly proportional to the area ratio of control. A new control scheme based only on sensing local streamwise wall shear stresses is devised with the aid of the genetic algorithm. A simple control scheme based on the difference of the streamwise wall shear stresses is found to reduce the wall skin friction considerably and alter the sublayer streaks drastically. In addition, a prototype feedback control unit for wall turbulence is developed and assessed with arrayed micro hot-film sensors and deformable shell magnetic actuators. Finally, some remaining important issues are discussed with an emphasis on the numerical and experimental synergetic strategy for future development of smart control of turbulence.

1. Introduction

It is well known that control of turbulent flows and associated transport phenomena should be a key in many engineering practices such as energy saving, efficient production process, securing high quality products, and resolving global environmental problems. Its impacts on future technology and human life would be enormous through manipulation and modification of turbulent drag, noise, heat transfer, mixing as well as chemical reaction. Our efforts are now directed toward innovating highly advanced control schemes and extending their application ranges.

A Japanese collaborative research project on "Smart Control of Turbulence: A Millennium Challenge for Innovative Thermal and Fluids Systems" was started in the fiscal year of 2000, and has reached its midway toward the final goal in the fiscal year of 2004. It is being supported through the Organized Research Combination System by the Ministry of Education, Culture, Sports, Science and Technology. Three national laboratories and several university laboratories are participating. As a part of their activity, a series of the Symposia on Smart Control of Turbulence is being held annually at the University of Tokyo.

†Also at Center for Smart Control of Turbulence, Maritime Research Institute, Tokyo 181-0004, JAPAN

In the above project, two major research areas have been identified; *i.e.*, advanced active control of turbulent shear flow and combustion. The control methodology includes development and application of microelectromechanical (MEMS) sensor/actuator devices, and introduction of additives such as micro bubbles and surfactant. The turbulent combustion control aims at reducing toxic emissions and stabilizing pre-mixed flames with some state feedback. The author and his colleagues are actively participating in the first research program, of which goal is to develop a feedback control unit for drag reduction in wall turbulence. This paper summarizes the recent progress in their effort, *i.e.*, software and hardware developments.

Among various control schemes, active feedback control is of great importance because of its potential to manipulate turbulent flows drastically with very small energy input (Moin & Bewley 1994; Gad-el-Hak 1996; Kasagi 1998). Choi *et al.* (1994) employed a so-called active cancellation method with local blowing/suction at the wall, which is based on the wall-normal velocity at $y^+ = 10$, and they obtained about 25% drag reduction in their direct numerical simulation (DNS) of turbulent channel flow. Bewley *et al.* (1993) applied a suboptimal control theory to turbulent channel flow, and obtained about 17% drag reduction. Recently, Lee *et al.* (1998) proposed a new suboptimal control algorithm based only on the wall variables such as the spanwise wall shear stress and the wall pressure fluctuations, whilst Lee *et al.* (1997) employed neural networks (NN) to predict the wall-normal velocity at a prescribed elevation from the spanwise wall shear stress, and they obtained about 20% drag reduction in their DNS of turbulent channel flow. Moreover, Endo *et al.* (2000) made DNS of channel flow control by assuming arrayed discrete wall sensors and deformable shell actuators, and found that such realistic arrayed units could lead to substantial drag reduction. Recently, by extending DNS to higher Reynolds numbers, Iwamoto *et al.* (2002) demonstrated that both active cancellation and suboptimal control schemes performed less in higher Reynolds number channel flows.

Most of the previous studies above have dealt with plane channel flows, while a circular pipe flow is another canonical wall-bounded flow and its control has several direct practical applications such as gas pipelines. Although control of pipe flow by rotation (Orlandi & Fatica 1997) and by rotational oscillation (Quadrio & Sibilla 2000) has been attempted with some degree of success, the wall actuation control mentioned above should also be tested. It is interesting to explore if the control algorithm proposed for channel flow is also effective for pipe flow. Therefore, in the first part of the present paper, the active cancellation control algorithm is applied to a turbulent pipe flow (Fukagata & Kasagi 2002b). Since, in reality, it may not be possible to have an entire wall surface equipped with an array of numerous active feedback control units, additional DNS is carried out for control applied only partially on a limited wall surface area.

In the previous DNS studies of active control algorithms for wall turbulence, the state feedback has been assumed to be made by sensing flow quantities that might be difficult to measure in practical flow system, *i.e.*, local spanwise wall shear stresses and spanwise wall pressure gradient. The former could be measured if a couple of sensors are employed, but the accuracy may not be sufficient owing to the diminishing scale of turbulence toward the wall, whilst the latter needs a new microfabrication technique. Hence, a control scheme based only on the streamwise wall shear stress, which is much easier to measure, is strongly desirable. In the second part of this paper, a genetic algorithm (GA) is introduced and tested to optimize the weights of sensor signals for triggering wall actuation (Morimoto *et al.* 2002). Although the optimal control is already applied to

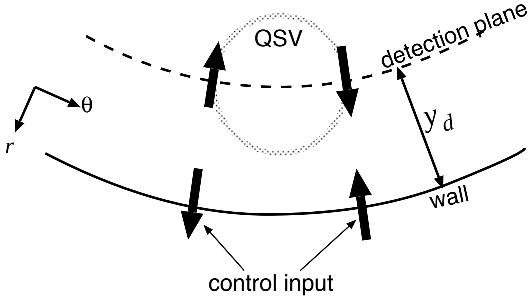

FIGURE 1. Active cancellation in pipe.

wall turbulence by Bewley *et al*. (2001), GA-based schemes have a potential to provide different control scheme in a much simpler form.

In the active feedback control schemes mentioned above, the near-wall coherent structures, which are primarily responsible for the turbulent transport mechanism (*e.g*., Robinson 1991; Kasagi *et al*. 1995), should be detected by sensors mounted on the wall, and selectively manipulated by the motion of actuators. Although the spatiotemporal scales of the coherent structures are generally very small, recent development of microelectromechanical systems (MEMS) technology has made it possible to fabricate flow sensors and mechanical actuators of submillimeter scale (*e.g*., Ho & Tai, 1996; Fujita, 1998). So, the third part of the paper describes the development of a prototype of feedback control system for wall turbulence with arrayed micro shear stress sensors and wall-deformation actuators, and the experimental assessment of its performance in a wind tunnel.

2. Active control of turbulent pipe flow

2.1 Numerical method

A computational code for DNS of turbulent pipe flow was developed based on a second-order accurate finite difference scheme on the cylindrical coordinate system. A special care was paid for consistency in the discretized space so that the energy is conserved by the inviscid part of the governing equation (Fukagata & Kasagi 2002a). The time integration was advanced by using the third order accurate Runge-Kutta/Crank-Nicolson (RK3/CN) scheme. Simulations were performed for two relatively low Reynolds numbers, $Re_b = 3050$ ($Re_\tau = u_\tau R / \nu \approx 110$) and $Re_b = 5300$ ($Re_\tau \approx 180$). It should be noted that in the case of $Re_b = 3050$ low-frequency intermittency was observed, which suggested that the flow remained in a transitional slug flow region. The statistics of an uncontrolled flow at $Re_\tau = 180$ computed by using the present code were in excellent agreement with previous DNS data by Eggels *et al*. (1994).

Throughout the present work, the mass flow rate, *i.e*., the bulk mean velocity U_b was kept constant. A fully developed turbulent flow is assumed in a circular pipe of a radius R, but the computation is made in a pipe of finite length L with periodic boundary conditions at both ends; $L = 35R$ and $40R$ for $Re_\tau = 110$ an 180, respectively. Thus, strictly speaking, the flow field should be always periodic in the streamwise direction, and it is particularly so in the case of partial area control.

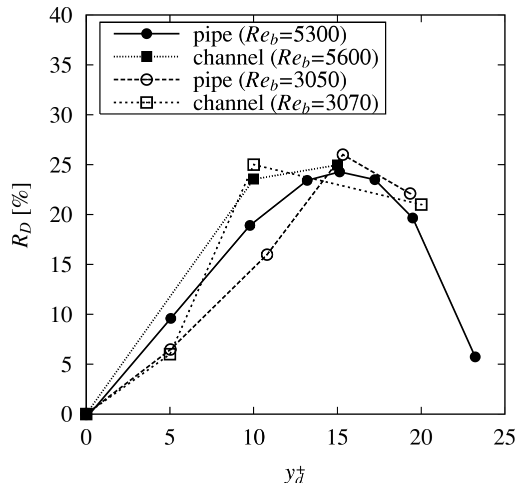

FIGURE 2. Drag reduction rate, R_D.

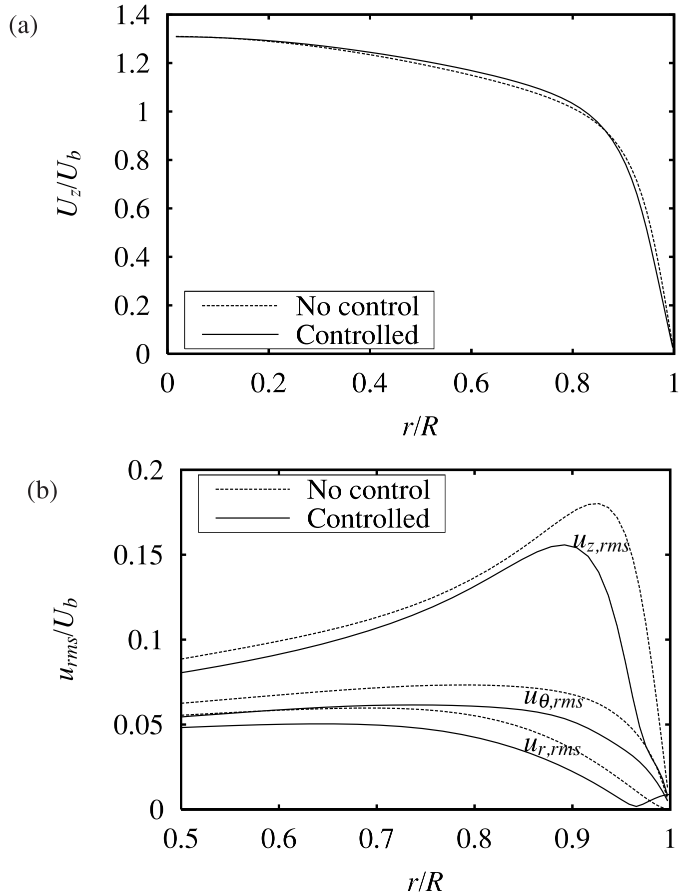

FIGURE 3. Velocity statistics of controlled flow at $Re_b = 5300$, $y_d^+ = 10$.
(a) Mean velocity, (b) rms velocity fluctuations.

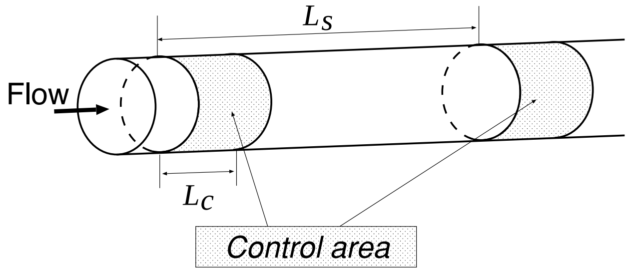

FIGURE 4. Schematic of partial control.

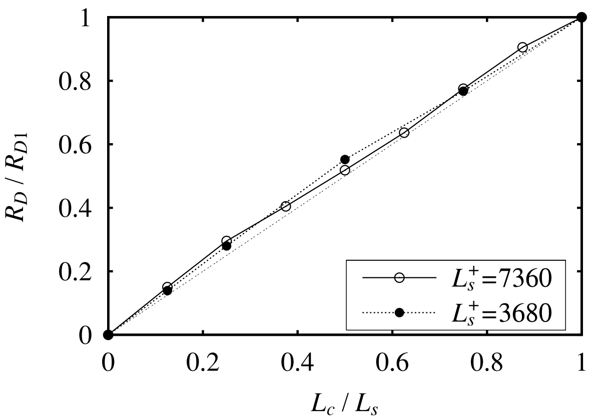

FIGURE 5. Drag reduction rate as a function of control length.

The control algorithm used in the present study is the so-called active cancellation control (v-control) of Choi *et al*. (1994), *i.e*.,

$$v_w = -u_r(y_d). \tag{2.1}$$

Here, y_d denotes the distance between wall and a virtual detection plane as shown in figure 1, and v_w is the radial velocity at the wall, *i.e*., $v_w = u_r|_{r=R}$.

2.2 DNS of pipe flow control

The investigation is initiated with active cancellation control applied on the entire wall with different locations of the detection plane, $y_d^+ = (R-r)^+ = 5$, 10, 15 and 20. Hereafter, superscript $^+$ is used for the dimensionless quantity normalized by the friction velocity of uncontrolled flow and the kinematic viscosity. Statistics shown below were obtained from the data accumulated over approximately 2000 wall unit time-span after the flow was judged to be in a quasi-steady state.

Figure 2 summarizes the relationship between y_d^+ and the drag reduction rate, $R_D = (C_{f0} - C_f)/C_{f0}$, where C_{f0} is the skin friction coefficient of the uncontrolled flow. Corresponding data for channel flow reported by Choi *et al*. (1994) are also plotted. The dependency of R_D on y_d^+ is similar to that in the channel flow. The maximum drag reduction is attained at $y_d^+ = 15$ for both Reynolds numbers presently specified. The magnitude of drag reduction rate is also comparable to that in the channel despite that

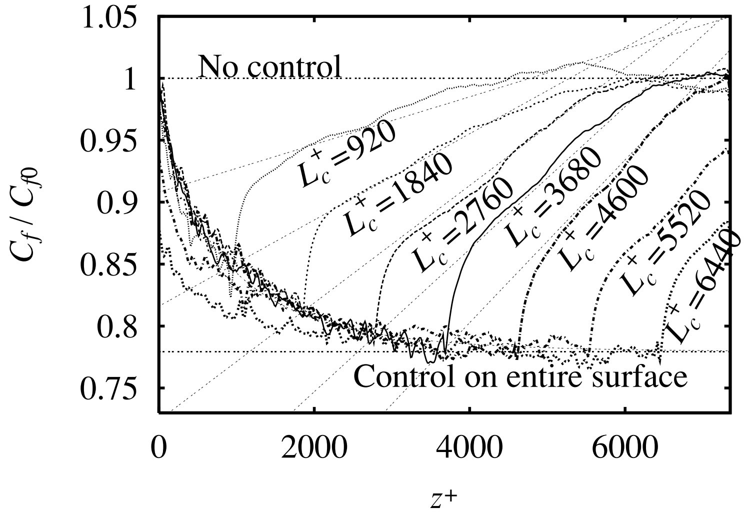

FIGURE 6. Normalized local skin friction coefficient for different control length.

the controlled surface area per volume of a pipe is twice as large as that of a channel.

Fundamental statistics of velocity and pressure are also calculated. As an example, mean and root-mean-square velocities are shown in figure 3. The mean velocity profile is slightly accelerated in the core region with the wall gradient reduced, while the three velocity fluctuation components are decreased. These changes in the statistics due to control are similar to those in the channel flow observed by Choi *et al*. (1994).

Simulation is continued with the control applied only in the region of $0 < z < L_c$ as shown in figure 4. Hereafter, only the case of $Re_b = 5300$ is considered and the detection plane is fixed at $y_d^+ = 10$. The separation length, L_s, is identical to the computational domain length, *i.e.*, $L_s^+ = L^+ = 7360$.

Figure 5 shows the drag reduction rate, R_D, as a function of L_c^+. Computed reduction rate is nearly proportional to the ratio of control length to separation length, *i.e.*, $R_D \approx (L_c/L_s)R_{D1}$, where R_{D1} is the drag reduction rate with the control on the entire wall. This result can be explained by the behavior of the local skin friction coefficient, $C_f(z)$, plotted in figure 6. The common behavior observed regardless of the value of L_c is as follows. In the controlled region, $C_f(z)$ decreases following a single curve. Just after the control ends, say in the region of $L_c^+ < z^+ < L_c^+ + 60$, the skin friction rapidly increases. Subsequently, $C_f(z)$ increases almost linearly up to the level of the uncontrolled flow. The endurance length of control effect after the end point of control is 2000-2500 wall units. The reason why such a rapid recovery process takes place right after the control is ceased remains to be explored, but anomalous pressure-strain correlation has been found to contribute to the substantial increase of the near-wall Reynolds shear stress.

3. Genetic algorithm for optimization of active control scheme

3.1 Genetic algorithm

Among four categories of control strategies (Gad-el-Hak 1996), GA-based control

(a)

(b)

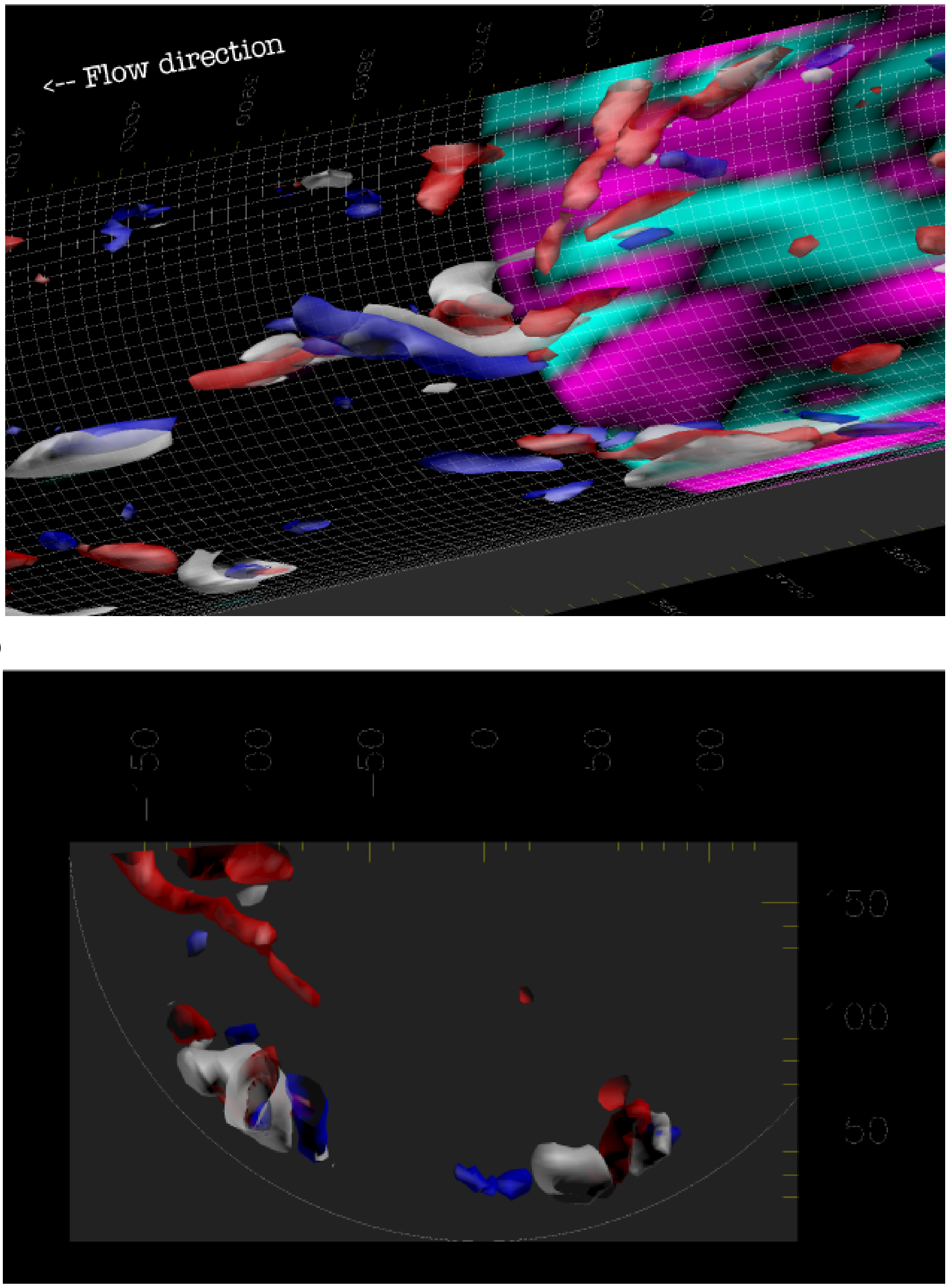

FIGURE 7. Instantaneous flow structure around the end point of control. (a) bird's-eye view; (b) cross-sectional view around $z^+ = 3700$. Isosurfaces: red, vortex with positive rotation ($Q^+ = -0.025$, $\omega_z > 0$); blue, vortex with negative rotation ($Q^+ = -0.025$, $\omega_z < 0$); white, high production ($P_{rz}^+ = 0.2$). Colors on the wall: magenta, blowing; cyan, suction.

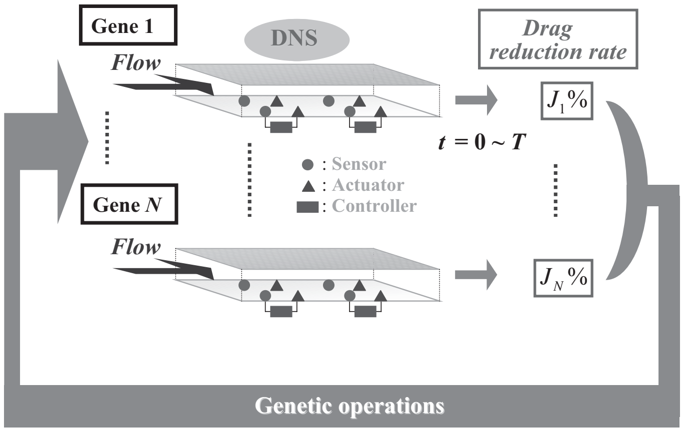

FIGURE 8. Schematic diagram of GA-based control.

algorithm is grouped into the adaptive scheme, in which control parameters are optimized through a training process with/without desired response of the controller. Once the control parameters are determined, the control input is readily calculated using algebraic equations. Therefore, GA-based control systems have an advantage in small computational load, since the time lag between sensing and actuation, which is crucial for stability of a control system, can be kept relatively short.

Genetic algorithm was derived from the evolution process of animals and plants, and is one of the optimization methods with random search (*e.g.*, Goldberg 1989). Basically, GA consists of three kinds of genetic operations: *selection*, *crossover* and *mutation*. Genes are evolved through these operations so as to maximize/minimize a prescribed cost function, and the optimal solution is found as a result of successive generation. GA attracts much attention because of its applicability to various kinds of optimization problems.

Figure 8 shows a schematic diagram of GA-based control. Control parameters to be optimized are transformed into genes, and N individuals including a set of genes are made. DNS using each individual is independently made and the cost function is calculated. Then, individuals giving smaller cost is statistically selected as parents, and two offsprings are made through crossover operation between them. In total, N children are created by applying the crossover operation $N/2$ times. Finally, mutations at a given rate are applied to all genes of N individuals. New generations are successively produced by repeating this procedure, and the optimal solution is obtained when the evolution has converged. In the present study, the cost function is set to be the wall skin friction averaged over a time period of 100 viscous time units.

3.2 Numerical procedure and control method

The numerical technique used in this study is almost the same as that of Kim *et al.* (1987); a pseudo-spectral method with Fourier series is employed in the streamwise (x) and spanwise (z) directions, while a Chebyshev polynomial expansion is used in the wall-normal (y) direction. A fourth-order Runge-Kutta scheme and a second-order Crank-Nicolson scheme are used for time advancement of the nonlinear terms and the viscous terms, respectively. The Reynolds number Re_τ, based on the wall friction velocity u_τ

and the channel half-width δ, is 100, and the bulk flow rate is kept constant. In order to reduce the computational load during optimization procedure using GA, the computational domain has a size of $1.25\pi\delta \times 2\delta \times 0.5\pi\delta$ in the x-, y-, and z- directions, respectively (hereafter, Domain I), with 16 × 65 × 16 spectral modes (in the x-, y-, and z-directions, respectively). When optimized control scheme is obtained, the computational domain is expanded to a larger size of $5\pi\delta \times 2\delta \times 2\pi\delta$ (hereafter, Domain II) with $64 \times 65 \times 64$ spectral modes in order to evaluate its performance. A fully developed flow field is used as an initial condition. During the optimization process, an instantaneous flow field of the unmanipulated channel in the previous generation is chosen as another initial flow field in the next generation in order to avoid convergence in a local optimum.

In the present study, wall blowing/suction is assumed to be a weighted summation of streamwise wall shear stresses measured with sensors aligned in the spanwise direction as follows:

$$v_w^+\left(x^+, z^+\right) = C\left(\sum_{n=-m}^{m} W_n \tau_w^+\left(x^+, z^+ + n\Delta z^+\right)\right) - \left\langle v_w^+ \right\rangle, \quad \tau_w^+ = \left.\frac{\partial u^+}{\partial y^+}\right|_w, \tag{3.1}$$

where W_n denote weights to be optimized, and $(2m+1)$ is the total number of the weights. The spanwise spacing between the virtual sensors Δz^+ is 6.5, which is the minimal grid spacing in the spanwise direction. The second term of the RHS of equation (3.1) denotes an ensemble average of v_w^+, which ensures the total sum of v_w^+ being zero at each time step, although its contribution is negligible.

Each W_n ($-1 < W_n < 1$) is expressed as a binary-coded string with 8 bits, and the weight distribution is determined through the optimization process described in the previous section. In the present study, the mutation rate is set to be 0.05. For evaluating the control effect under constant energy input, the constant C in equation (3.1) is separately determined at each time step in such a way that the root-mean-square value of v_w^+ is 0.15, which is almost the same as the rms value of v^+ at $y^+ = 10$ in the unmanipulated channel.

3.3 Weight distribution

In order to obtain convergent solutions efficiently, two modes for W_n are defined as follows:

$$\begin{cases} W_0 = 0, \;\; W_{-n} = -W_n \;(n = 1,2,3) \\ 0 \le W_1 \le 1, \;\; -1 \le W_n \le 1 \;(n = 2,3) \end{cases} \quad \text{(Mode 1)} \tag{3.2}$$

$$\begin{cases} W_{-n} = W_n \\ -1 \le W_n \le 1 \end{cases} (n = 0,1,2,3) \quad \text{(Mode 2)} \tag{3.3}$$

where Modes 1 and 2 are weight distributions which are antisymmetric and symmetric in the spanwise direction, respectively. In the present study, m in equation (3.1) is set to be 3, so that the spanwise extent of the sensor array is about 40 (ν/u_τ), which is slightly smaller than half the mean spacing of streaks.

Figure 9 shows the evolution of the maximum drag reduction rate in each generation.

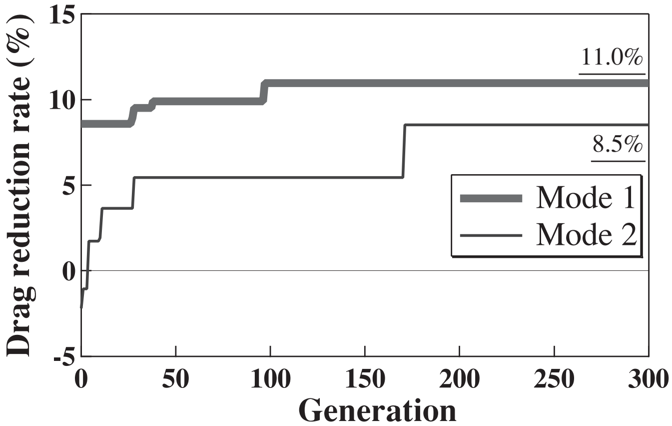

FIGURE 9. Evolution of drag reduction rate.

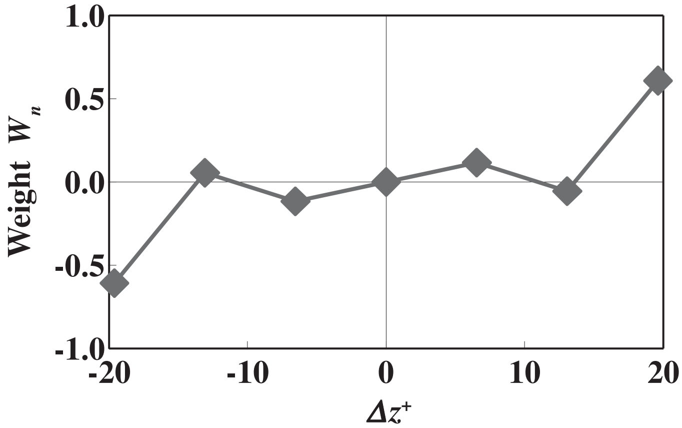

FIGURE 10. Weight distribution optimized by GA.

The drag reduction of about 11% and 8.5% is achieved after 97 and 171 generations in Modes 1 and 2, respectively. The population size N, that is, the number of individuals evaluated at each generation, is 60 and 30, respectively, so that the total number of DNSs until the convergent solution is obtained, $G \times N$, is 5000 ~ 6000 for both modes. Since larger drag reduction is obtained in Mode 1 than in Mode 2, the discussion hereafter is focused on the result of Mode 1.

Figure 10 shows the optimized weight distribution, where W_n at $\Delta z^+ = \pm 19.5$ have large absolute values, while others in the range of $-13 < \Delta z^+ < 13$ are almost zero. Therefore, the control input is almost proportional to the spanwise differential of the streamwise wall shear stresses about ± 20 (ν/u_τ) apart in the spanwise direction from actuators. From this result, the most efficient control input can be written in the following simple form:

$$v_w = C\left\{\tau_w\left(x^+, z^+ + 20\right) - \tau_w\left(x^+, z^+ - 20\right)\right\}. \tag{3.4}$$

The Fourier representation of the above equation is

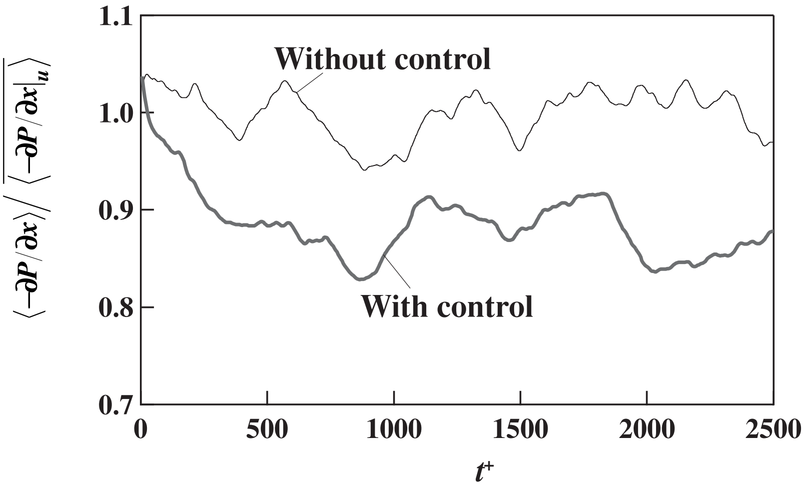

FIGURE 11. Time histories of pressure gradient.

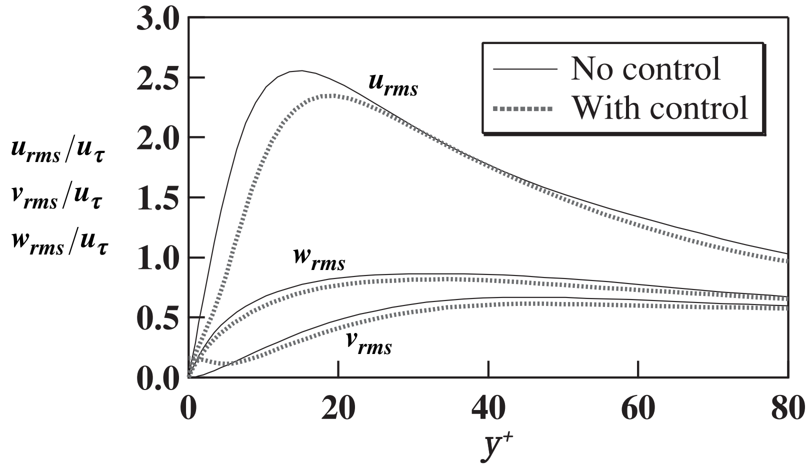

FIGURE 12. Root-mean-square velocity fluctuations.

$$\hat{v}_w(k_x, k_z) = C\left\{ i \sin\left(\frac{k_z}{16}\pi\right)\right\} \cdot \hat{\tau}_w(k_x, k_z), \tag{3.5}$$

where the hat denotes the Fourier coefficient, and k_x and k_z the streamwise and spanwise wave numbers in the x- and z- directions, respectively. From equation (3.5), one can expect that the phase of v_w is $\pi/2$ ahead of that of τ_w regardless of k_x or k_z , and the magnitude of v_w is most sensitive to τ_w when k_z equals to 8. Note that the wavelength of the wave of $k_z = 8$ corresponds to about 80 (ν/u_τ) in the physical space, which is close to the spacing of the streaky structures most frequently observed.

3.4 Control performance and drag reduction mechanism

We applied the control scheme given in equation (3.4) to a larger computational do-

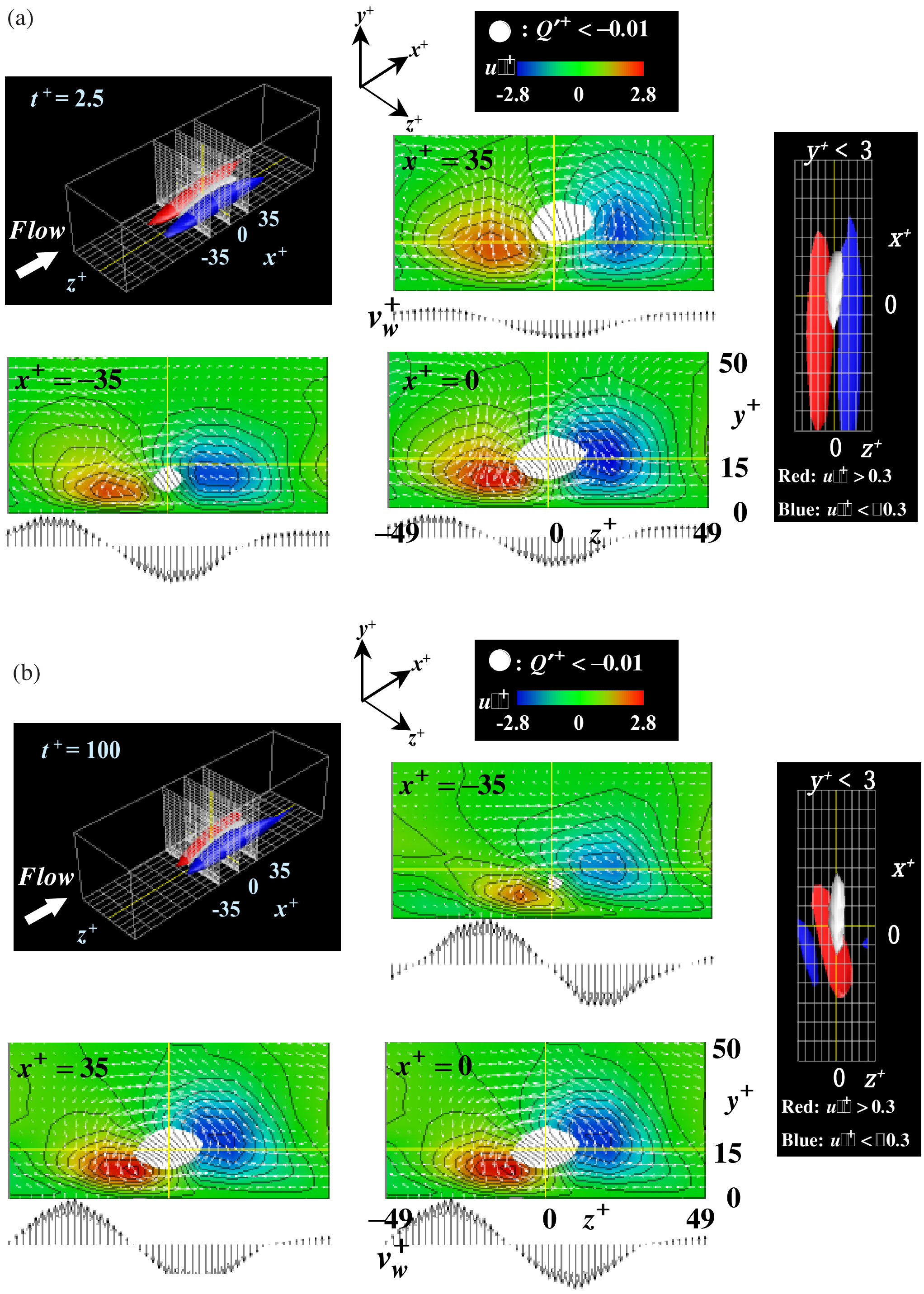

FIGURE 13. Conditionally-averaged flow field and control input. Velocity vectors, iso-contours of u'^+ and isosurfaces of the second invariant of the deformation tensor ($Q^+ < -0.01$): (a) $t^+ = 2.5$, (b) $t^+ = 100$.

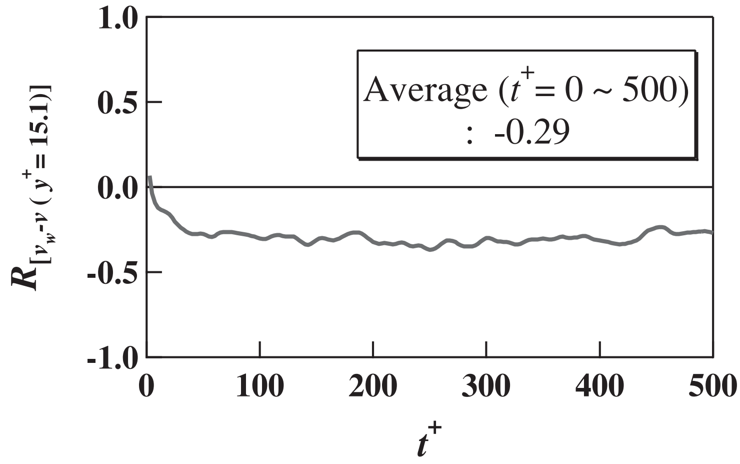

FIGURE 14. Time history of the correlation coefficient of v_w and v at $y^+ = 15.1$.

main (Domain II) in order to evaluate its efficiency and examine its effect on turbulent structures. Figure 11 shows the time histories of the pressure gradient normalized by the time-averaged pressure gradient of the unmanipulated channel. The skin friction decreases drastically once the control starts, and the maximum drag reduction rate of about 18% is obtained. The mean drag reduction rate during the period $t^+ = 0 \sim 2500$ is about 12%. The rms velocity fluctuations in the wall coordinates are shown in figure 12. As in figure 3 (b), turbulent intensities are significantly reduced by the control.

It is now clear that we could achieve significant drag reduction with the present control scheme, which gives a spanwise antisymmetric distribution of the control input as in figure 10. In order to investigate the present drag reduction mechanism, we examine the relationship between control input v_w and near-wall streamwise vortices below. With a conditional averaging technique based on the second invariant of the deformation tensor ($Q^+ < -0.01$) at $y^+ = 14.3$, the near-wall streamwise vortices are sampled. Instantaneous flow fields surrounding detected points are spatially-averaged keeping the sign of streamwise vorticity. The conditionally-averaged flow field with $\omega_x < 0$ is represented in figure 13. The flow field just after the onset of control ($t^+ = 2.5$) is shown in figure 13 (a), where the flow field has not been much modified by the control input yet. As can be conjectured from equation (3.4), the control input becomes largest at the boundary between high and low speed regions near the wall, which is located beneath a streamwise vortex. Namely, blowing is applied to the vortex with $\omega_x > 0$, while suction is applied to that with $\omega_x < 0$.

Figure 13 (b) shows the conditionally-averaged flow field at $t^+ = 100$, which must have been cumulatively affected by the wall blowing/suction. It is found that the streamwise velocity distribution is drastically modified in the vicinity of the wall, and hence the relative locations of the control input and the streamwise vortex are also changed, especially around the leg region of a vortex. Blowing beneath the streamwise vortex decelerates the flow and shifts the boundary between low and high speed streaks in the spanwise direction. On the other hand, suction accelerates the flow near the wall, but also moves the boundary in the same spanwise direction. The degree of this spanwise shift of the boundary adjacent to the wall depends on the wall elevation of the streamwise vortex, so that the boundary is tilted in the spanwise direction as noticed in the plane

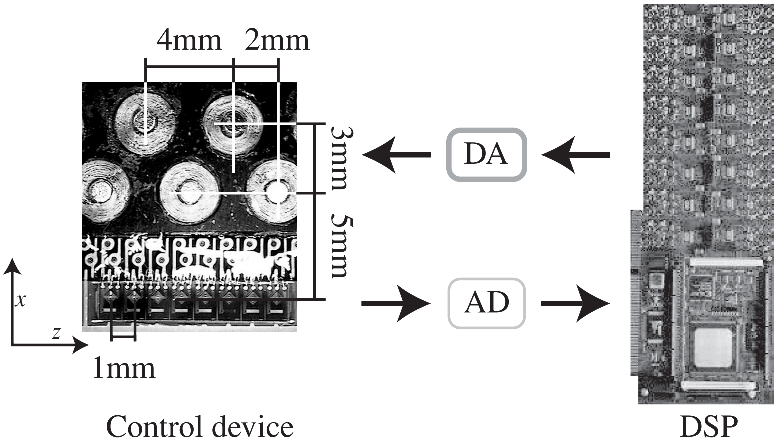

FIGURE 15. Prototype system for wall turbulence control with arrayed sensors and actuators.

view of figure 13 (b). As a result of this shift, the control input becomes almost 180 degree out-of-phase with the wall-normal velocity induced by the streamwise vortex.

Figure 14 shows the time history of the correlation coefficient between v_w and v at $y^+ = 15.1$. It is observed that the coefficient becomes negative with time and remains almost constant at about -0.3. Therefore, the control rule reached by the present GA gives a control input distribution similar to that of v-control (Choi *et al*. 1994), although the present scheme requires only sensing the streamwise wall shear stress.

4. Development of active feedback control unit

4.1 Control system description

In the present work, hot-film sensors are employed for the measurement of the streamwise wall shear stress, while magnetic wall-deformation actuators are used to introduce control input into the flow field. A single row of eight hot-film sensors with a spanwise spacing of 1 mm are used as shown in figure 15. Two rows of arrayed actuators with a 4 mm spacing are arranged with a 2 mm offset in the spanwise direction, and consequently five actuators are located with a 2 mm spanwise spacing. These spanwise spacings of the sensors and actuators are about 10 and 20 wall units under the experimental flow condition described later, respectively. A digital signal processor (DSP) board (SMT-326, Sundance DSP Inc.) with 32 channel analog inputs and outputs is used. The output voltage of the circuit for the constant temperature hot-film sensor is first digitized by a 16-bit AD converter. The control signal for the actuator is then computed with a DSP (C44, 60MFLOPS) and converted back to an analog signal through a 16-bit DA converter. The present DSP system has an inherent time delay of 1.6 ms for data transfer and processing.

4.2 Micro wall shear stress sensor

A schematic of the micro shear stress sensor used is shown in figure 16. A platinum thin-film heater is deposited on a Si_3N_4 diaphragm of 1 μm in thickness and 400×400 μm^2 in area. In order to keep a sufficiently large electric resistance of the heater, the thin

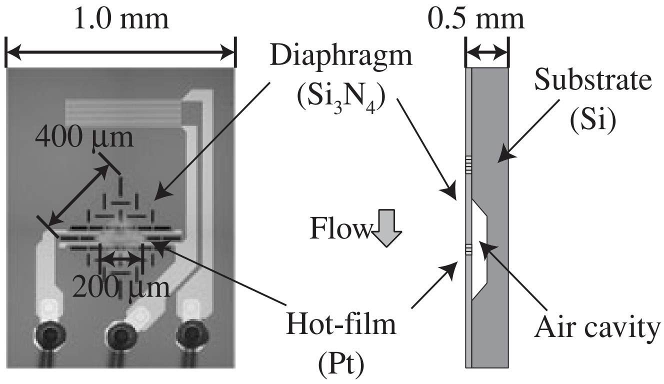

FIGURE 16. Magnified view of micro hot-film shear stress sensor.

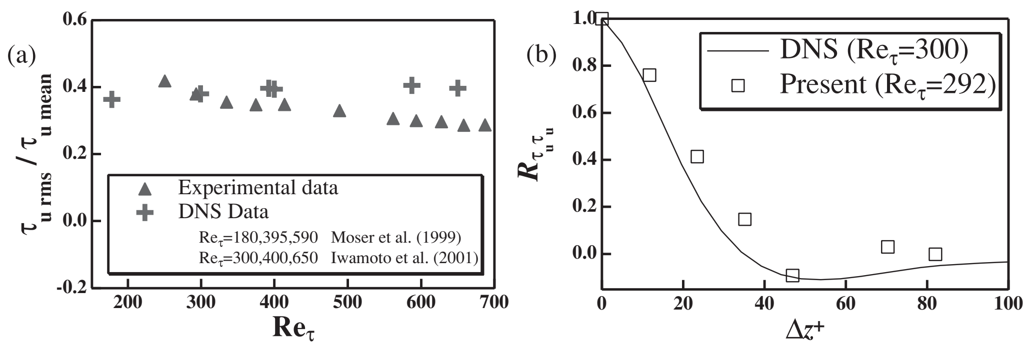

FIGURE 17. Wall shear stress measurement.
(a) Root-mean-square wall shear stress fluctuations, (b) spanwise two-point correlation.

heater is patterned zigzag in an area of 200×23 μm^2. An air cavity of 200 μm in depth is formed underneath the diaphragm for reducing heat loss to the substrate. Another platinum resistor is made on the substrate and used for temperature compensation.

Figure 17 (a) shows the root-mean-square wall shear stress fluctuation $\tau_{u\ rms}$. It is found in DNS studies (*e.g.*, Moser *et al.* 1999; Iwamoto *et al.* 2001) that $\tau_{u\ rms}$ is weakly dependent on the Reynolds number when it is normalized by the mean wall shear stress $\tau_{u\ mean}$, and $\tau_{u\ rms}/\tau_{u\ mean}$ is equal to 0.36-0.4. The present results in a fully developed turbulent air channel flow show that the measured data decreases with increasing the Reynolds number owing to an insufficient frequency response of the sensor, although the signal deterioration is negligible at $Re_\tau<400$.

The spanwise two-point correlation of τ_u obtained with the arrayed sensors is shown in figure 17 (b). The present data shows a negative peak at $\Delta z^+ \sim 50$, and is in good accordance with the DNS data. Therefore, the near-wall coherent structures, which are the target of the feedback control, can be well captured with the present wall shear stress sensors.

4.3 Deformable shell actuators

Figure 18 shows a schematic of deformable shell magnetic actuator. An elastic mem-

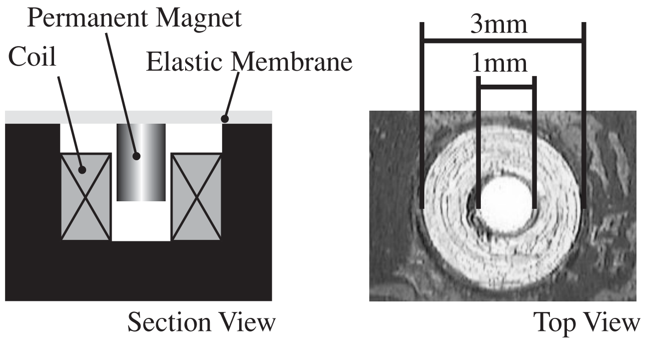

FIGURE 18. Schematic of magnetic deformation actuator.

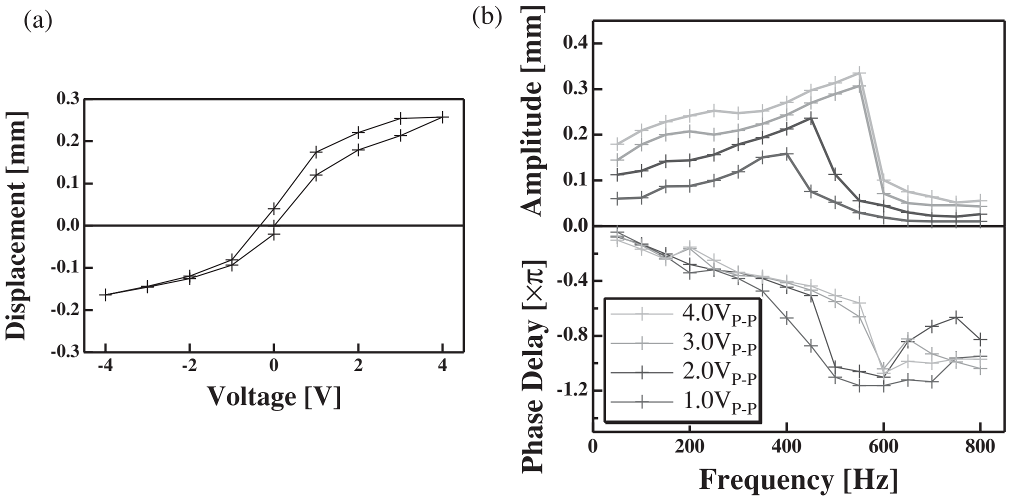

FIGURE 19. Characteristics of magnetic deformation actuator.
(a) Static response, (b) dynamic response.

brane made of silicon rubber of 0.1 mm in thickness is used, and a rare-earth miniature permanent magnet of 1 mm in diameter is glued on the membrane backside. A miniature copper coil (500 turns), of which outer diameter is 3 mm, is placed underneath the magnet. The static and dynamic response characteristics of the actuator are shown in figure 19 (a) and (b). The displacement is a nonlinear function of the static voltage applied, and about 100 μm with an imposed voltage of 4V. The dynamic response is dependent on the amplitude of the imposed voltage, because the spring constant of the membrane is increased with increasing the deformation as shown in figure 19 (a). Hence, the resonant frequency is increased from 450 to 600 Hz when the amplitude is increased from 1 to 4 V. The time interval required for the control described later is about 5 ms, so that the frequency response of the actuator should be satisfactory.

The effect of the deformable actuator on the fluid is examined in a quiescent air chamber ($160 \times 160 \times 160$ mm^3). Figure 20 (a) shows an instantaneous tracer picture near the actuator driven with a 400 Hz sinusoidal signal. It is seen that, when the actuator reaches its maximum height of 200 μm, its shape looks like a frustum, and the fluid is radiated

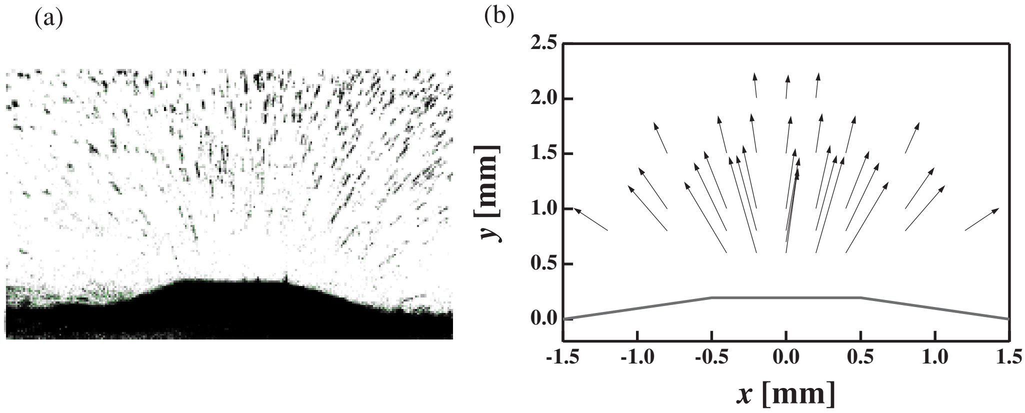

FIGURE 20. Velocity field around deformation actuator.
(a) Flow visualization, (b) LDV measurement.

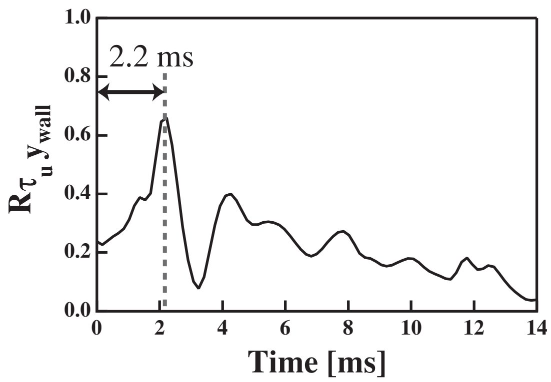

FIGURE 21. Correlation coefficient of streamwise shear stress fluctuation and actuator displacement.

from the top surface of the actuator. The flow induced is also measured with a 2-component laser Doppler velocimeter (Dantec Dynamics Inc., 60X61). The phase-averaged velocity vectors are shown in figure 20 (b). The maximum fluid velocity obtained at the elevation twice the maximum displacement of the actuator is about 0.25 m/s, which is about half of the maximum wall velocity.

4.4 Assessment of prototype control unit

The present prototype system is evaluated in a rectangular wind duct. The channel width and height are 50 and 500 mm, respectively. The test section is located 80H downstream from the inlet, where the flow is fully-developed. The bottom wall is equipped with the control system described above. The bulk mean velocity U_b is varied from 2.5 to 9.3 m/s, which corresponds to the Reynolds number Re_τ based on the wall friction velocity u_τ and the channel half-width from 250 to 800. When $Re_\tau = 300$ ($U_b = 3.0$ m/s), viscous length and time units correspond to 0.09 mm and 0.5 ms, respectively. Under this flow condition, the mean diameter of the near-wall coherent streamwise vortex is

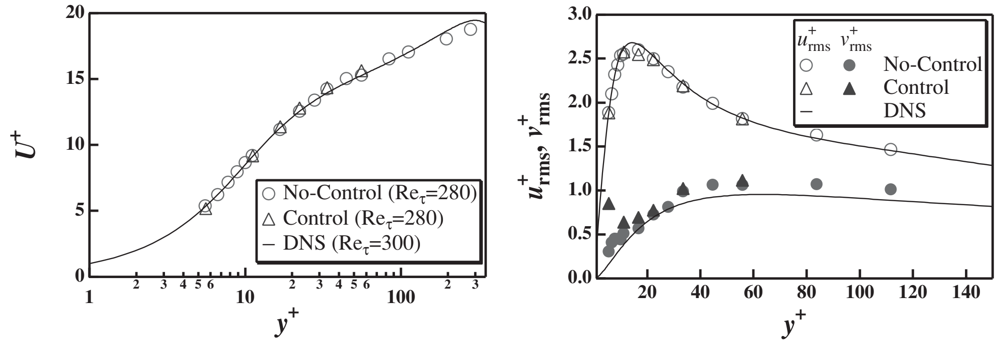

FIGURE 22. Velocity measurement above the actuator in turbulent channel flow. (a) Streamwise mean velocity, (b) streamwise and wall-normal rms velocity fluctuations.

estimated to be about 2.7 mm (~30 ν/u_τ), while it takes a time length of about 5 ms (~10 ν/u_τ^2) for a vortex to travel over a fixed wall-sensor.

The dynamic response of the entire control system shown in figure 15 is assessed with a simple feedback scheme. Namely, the actuator is driven by a signal, which is supplied through the DPS in proportion to the instantaneous wall shear stress fluctuation measured by the sensor. The deformation of the actuator is continuously measured with a laser displacement meter. Figure 21 shows the cross correlation coefficient of the shear stress fluctuation and the actuator displacement. It is evident that the correlation has a clear maximum, which indicates that the present system has an internal time delay of 2.2 ms between sensing the stress and driving the actuator. Since the temporal persistence of the streamwise vortex is about 5 ms as mentioned above, the present control system should be effective in manipulating many of the passing vortices. It is noted that most of the time delay is caused by the DSP itself. A faster controller using a field programmable gate array (FPGA) having 256 analog input/output channels is now being developed. With this FPGA, the inherent time delay of the controller will be much decreased to less than 0.2 ms, so that the total control time delay would be 0.8 ms.

In order to find the effect of the present control with the simple feedback rule preliminarily, the streamwise and wall-normal velocity fluctuations manipulated by the deformable shell actuator are measured. To do this, a two-component LDV system using three laser beams is employed; the diameter of the beam is 1.35 mm and the focal length of the lens is 400 mm, while the measurement volume is about 190 × 190 × 5500 μm^3. As tracers, smoke particles of about 1 μm in diameter, which are generated by the SAFEX® fog generator (Dantec Dynamics Inc., FOG 2010), are introduced into the wind tunnel.

The results are represented in figure 22. The streamwise mean velocity profiles of both unmanipulated and manipulated flows are in good agreement with the DNS result (Iwamoto *et al.* 2002), so that there is no observable effect on the mean flow field. In figure 22 (b), the wall-normal velocity fluctuation is significantly increased near the wall owing to the motion of actuator, although the streamwise component is unaffected. Note that the magnitude of induced v_{rms} is much larger than that assumed in the previous DNS studies for active control of wall turbulence (see, *e.g.*, figure 3 (b)).

Figure 23 shows a magnetic MEMS actuator cluster recently developed. It has lined tiny flaps, which swing on hinges. The flap is made of polyimide, and its area of about 1 × 2 mm^2 is much smaller than the actuator in figure 18. With this seesaw configura-

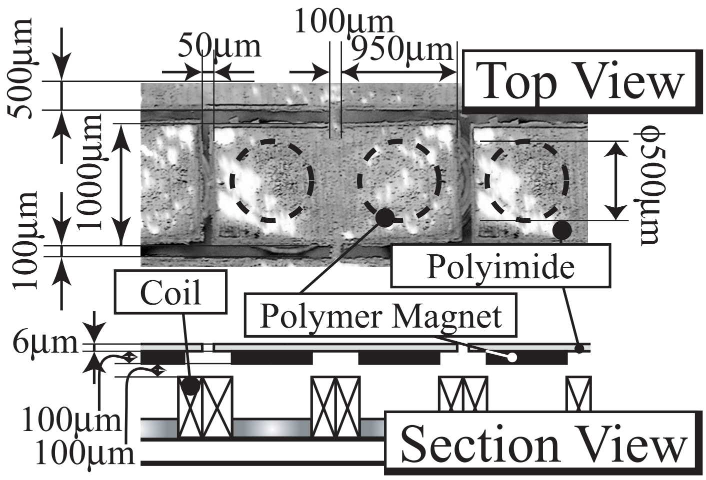

FIGURE 23. Prototype of MEMS magnetic actuators.

tion, large displacement as well as high frequency response can be achieved. A permanent polymer magnet is formed on the backside of the flap, and it is driven by the magnetic force induced by a miniature coil underneath. So far, the displacement of the prototype is about 10 µm, and it should be improved by tuning the fabrication process.

4. Concluding remarks

The present paper has concentrated on the recent progress in the active feedback control of wall-bounded turbulence, which has been made by the author's group at the University of Tokyo as a part of the collaborative project on "Smart Control of Turbulence" in Japan. Both hardware and software to be integrated in a future control unit have been intensively studied and developed. That is, the direct numerical simulation has been extensively used to assess conceived control algorithms and explore the turbulence mechanism modified by a control. With the rapid advancement in hardware, the control schemes suitable for real applications, *e.g.*, adaptive schemes, have been identified increasingly worth studying in addition to more ideal schemes such as optimal and dynamical systems control schemes. The micro fabrication technology has also been introduced and exploited for producing arrayed small-scale sensors/actuators and high performance field programmable gate array units.

In order to highlight the progress, three studies are briefly described. First, the active cancellation control is tested in DNS of turbulent pipe flow. The simulation is made with the control applied on the wall entirely and partially. It is found that the drag reduction rate achieved is comparable to that in the plane channel flow (~25 %), and that, when partially controlled, the reduction rate is nearly proportional to the area ratio of control. It is also found that the flow recovers to the uncontrolled state within an about 2000 - 2500 wall unit length downstream of the end of control.

A new control scheme based only on sensing the local streamwise wall shear stresses is devised with the aid of the genetic algorithm; its performance is again evaluated through direct numerical simulation of turbulent channel flow. As a result, the control scheme, in which the control input given by the actuator is proportional to the difference of the streamwise wall shear stresses about ±20 (ν/u_τ) apart in the spanwise direction, is found to reduce the wall skin friction as much as 18%. The streaky structures in the vicinity of the wall are drastically altered by the control, and this leads to the control input which opposes the wall-normal velocity components associated with the near-wall vortices.

Finally, the prototype of the feedback control unit for wall turbulence is developed with arrayed micro hot-film sensors and deformable shell magnetic actuators. The dynamic responses of the sensors and actuators are found to be sufficiently high for the experimental condition employed. The time delay of the feedback loop of the prototype system is estimated to be 2.2 ms, to which the digital signal processor is a major contributor. The LDV measurement shows that the actuator can introduce sufficiently large control input to the flow field.

There are yet difficult, but important issues that should be resoled to develop a real control system in the future. Even more efforts should be made to study control algorithms to achieve higher control performance even at higher Reynolds numbers. In the case of the pipe flow control above, for example, the drag reduction rate is just proportional to the area of control, but we should find a scheme with which we can obtain excessively larger drag reduction with fractional control. It is known that, at higher Reynolds numbers, most of the control schemes work less effectively (Iwamoto *et al.* 2002). It is because the turbulence activity farther from the wall is making larger contribution to the wall skin friction as the Reynolds number increases, and some new control methodology should be proposed for preventing the nonlinear interaction between the sublayer and log-region structures. The control algorithm, however, should be simple enough, since we cannot afford increasing data processing load which results in the high cost of controller. Developing durable and effective sensors and actuators should also be accelerated while keeping them cost effective. This will be plausible with the rapid spread of MEMS technology into the scientific research community, but hopefully further development of MEMS-based controller units integrating micro sensors, micro actuators and CPUs should be led by careful and precise numerical simulations and assessment. Thus, there is no doubt that the numerical and experimental synergetic strategy will be even more important for future development of smart control of turbulence.

The author is deeply indebted to Drs. Y. Suzuki, K. Fukagata and T. Endo, and also Messrs. K. Iwamoto, T. Yoshino, K. Morimoto and M. Tsuda for their work described herein

REFERENCES

BEWLEY, T., CHOI, H., TEMAM, R. & MOIN, P. 1993 Moin: Optimal feedback control of turbulent channel flow. *CTR Annual Research Briefs-1993,* pp. 3-14. Center for Turbulence Research, Stanford Univ./NASA Ames Research Center.

BEWLEY, T., MOIN, P. & TEMAM, R. 2001 *J. Fluid Mech.* **447**, 179-.

CHOI, H., MOIN, P. & KIM, J. 1994 Active turbulence control for drag reduction in wall bounded flows. *J. Fluid Mech.* **262**, 75-110.

EGGLES, J. G. M., UNGER, F., WEISS, M. H., WESTERWEEL, J., ADRIAN, R. J., FRIEDRICH, R. & NIEUWSTADT, F. T. M. 1994 Fully developed turbulent pipe flow: a comparison between direct numerical simulation and experiment. *J. Fluid Mech.* **268**, 175-209.

ENDO, T., KASAGI, N. & SUZUKI, Y. 2000 Feedback control of wall turbulence with wall deformation. *Int. J. Heat Fluid Flow* **21**, 568-575.

FUJITA, H. 1998 Microactuators and micromachines *Proc. IEEE* **86**, 1721-1732.

FUKAGATA, K. & KASAGI, N. 2002a Highly energy-conservative finite difference method for cylindrical coordinate system. *J. Comput. Phys.* submitted.

FUKAGATA, K. & KASAGI, N. 2002b Active feedback control of turbulent pipe flow. *Proc. 3rd Symposium on Smart Control of Turbulence, March 2002, Tokyo,* pp. 99-105. Center for Smart Control of Turbulence, NMRI.

GAD-EL-HAK, M. 1996 Modern developments in flow control. *Appl. Mech. Rev.* **49**, 365-379.

GOLDBERG, D. E. 1989 *Genetic algorithms in search, optimization and machine Learning*. Addison-Wesley.

HAMILTON, J. M., KIM, J. & WALEFFE, F. 1995 Regeneration mechanism of near-wall turbulence structures. *J. Fluid Mech.* **287**, 317-348.

HO, C.-M. & TAI, Y.-C. 1996 Review: MEMS and its applications for flow control. *ASME J. Fluids Eng.* **118**, 437-447.

IWAMOTO, K., SUZUKI, Y. & KASAGI, N. 2002. Reynolds number effect on wall turbulence: toward effective feedback control. *Int. J. Heat Fluid Flow* to appear.

JIANG, F., TAI, Y.-C., GUPTA, B., GOODMAN, R., TUNG, S., HUANG, J.-B. & HO, C.-M. 1996 A surface-micromachined shear stress imager. *Proc. IEEE Workshop on MEMS*, *February 1996, San Diego,* pp. 110-115, IEEE.

KASAGI, N. 1998 Progress in direct numerical simulation of turbulent transport and its control. *Int. J. Heat Fluid Flow* **19**, 128-134.

KASAGI, N., SUMITANI, Y., SUZUKI, Y. & IIDA, O. 1995 Kinematics of the quasi-coherent vortical structure in near-wall turbulence. *Int. J. Heat Fluid Flow* **16**, 2-10.

KIM, J., MOIN, P. & MOSER, R. 1987 Turbulence statistics in fully developed channel flow at low Reynolds number. *J. Fluid Mech.* **177**, 133-166.

LEE, C., KIM, J., BABKOCK, D. & GOODMAN, R. 1997 Application of neural network to turbulence control for drag reduction. *Phys. Fluids* **9**, 1740-1747.

LEE, C., KIM, J. & CHOI, H. 1998 Suboptimal control of turbulent channel flow for drag reduction. *J. Fluid Mech.* **358**, 245-258.

MOIN, P. & BEWLEY, T. 1994 Feedback control of turbulence. *Appl. Mech. Rev.* **47**, S3-S13.

MORIMOTO, K., IWAMOTO, K., SUZUKI, Y. & KASAGI, N. 2002 Generic algorithm-based optimization of feedback control scheme for wall turbulence. *Proc. 3rd Symposium on Smart Control of Turbulence, March 2002, Tokyo,* pp. 107-113. Center for Smart Control of Turbulence, NMRI.

MOSER, R. D., KIM, J. & MANSOUR, N. N. 1999 Direct numerical simulation of turbulent channel flow up to $Re_\tau = 590$. *Phys. Fluids* **11**, 943-945.

ORLANDI, P. & FATICA, M. 1997 Direct simulations of turbulent flow in a pipe rotating about its axis. *J. Fluid Mech.* **343**, 43-72.

QUADRIO, M. & SIBILLA, S. 2000 Numerical simulation of turbulent flow in a pipe oscillating around axis. *J. Fluid Mech.* **424**, 217-241.

ROBINSON, S. K. 1991 Coherent motions in the turbulent boundary layer. *Annu. Rev. Fluid Mech.* **23**, 601-639.

YOSHINO, T., TSUDA, M., SUZUKI, Y. & KASAGI, N. 2002 Toward development of feedback control system for wall turbulence with MEMS sensors and actuators. *Proc. 3rd Symposium on Smart Control of Turbulence, March 2002, Tokyo,* pp. 115-120. Center for Smart Control of Turbulence, NMRI.